AN ABSTRACT OF THE THESIS OF

Kent C. Bostick for the degree of Master of Science in Nuclear Engineering presented on February 4, 1992. Title: A Two-Dimensional Temperature Model for Target Materials Bombarded by Ion Beams.

Redacted for Privacy

Abstract approved: ______________________________
Andrew C. Klein

The ion implantation process is a very precise, controllable, and reproducible method used to enhance material properties of finished components such as ball bearings. Essentially, the target material is bombarded by accelerated ions to form a thin alloyed layer in the substrate. As the ions deposit their kinetic energy in the target it begins to heat up. To prevent thermal distortion in the finished pieces the ion implantation is performed at dose levels (dependent on the ion fluence and time duration of implantation) to insure that the target pieces stay at relatively low temperatures. Consequently, the low temperature requirement for many applications limits the economic, and probably, the physical success of ion implantation.

The purpose of this study was to show the applicability of using a two-dimensional computer code developed to model plasma disruptions and subsequent energy deposition on a fusion reactor first wall to calculate surface and bulk temperature information during ion implantation. In

turn the code may assist researchers pursuing development of adequate cooling for target materials in an attempt to overcome the low temperature constraint.

All data supported the hypotheses that the two-dimensional code previously developed for fusion reactor applications was adequate to model the ion implantation process.

A Two-Dimensional Temperature Model for Target Materials Bombarded by Ion Beams

by

Kent C. Bostick

A THESIS

submitted to

Oregon State University

in partial fulfillment of
the requirements for the
degree of

Master of Science

Completed February 4, 1992

Commencement June 1992

APPROVED:

Redacted for Privacy

Professor of Nuclear Engineering in charge of major

Redacted for Privacy

Head of department of Nuclear Engineering

Redacted for Privacy

Dean of Graduate School

Date thesis presented February 4, 1992

Typed by Kent C. Bostick for Kent C. Bostick

ACKNOWLEDGEMENT

I wish to acknowledge Dr. Ahmed Hassanein of Argonne National Laboratory for the use of his computer code, ATHERMAL*2, which made this entire project possible. I would also like to acknowledge his continued support throughout this process. Additionally, I wish to thank Dr. Alan Robinson of Oregon State University for his help with the one-dimensional modeling.

The contributions of my advisor, Dr. Andrew Klein, were many and greatly appreciated. First, I will thank him for serving as an advisor that always had an encouraging word and an interest in my progress. I also appreciate the timely reading and return of various rough drafts. Furthermore, I would like to express by appreciation for all the logistics help these past few weeks. Without his continued support and guidance over the years, this project may never have been completed.

I also wish to acknowledge the support of family and friends. To John and Betty Garber, whose computer kept the research light from completely being extinguished, and to my father, Ken Bostick, and my mother, Pat Bostick, for their moral and financial support throughout the years. Finally, I wish to thank Ann Adams for her tremendous support these past couple of years.

TABLE OF CONTENTS

I.	INTRODUCTION	1
II.	HEAT BUILD-UP DURING ION IMPLANTATION	5
III.	NUMERICAL SOLUTION OF THE PARTIAL DIFFERENTIAL EQUATION	7
	III.A. Implicit Crank-Nicolson Approximations	8
	III.B. Initial Condition	13
	III.C. Boundary Conditions	13
IV.	ATHERMAL*2	18
	IV.A. Input Parameters	19
	IV.B. Surface Heat Flux	19
V.	CALCULATIONS	24
	V.A. The Sampath and Wilbur Experiment	24
	V.B. Modeling Approximations	26
	V.C. Source Input	29
	V.D. Results	30
VI.	CONCLUSION	41
REFERENCES		43

LIST OF FIGURES

Figure		Page
1.	Depiction of Boundary Conditions	14
2.	Insulated Boundary Condition	16
3.	Surface Condition	16
4.	Schematic Illustrating Ion Beam - Target Interaction	21
5.	Schematic of Implantation System	25
6.	Target Holder to be Modeled	27
7.	Cylindrical Geometry Approximation for Target Holder	28
8.	Centerline Surface Temperature (11 sec. deposition)	32
9.	Radial Surface Temperature Distribution (11 sec. deposition)	34
10.	Radial Surface Temperature Distribution: Various Beam Radii (11 sec. deposition)	36
11.	Centerline Surface Temperature (17 sec. deposition)	39
12.	Radial Surface Temperature Distribution (17 sec. deposition)	40

A TWO-DIMENSIONAL TEMPERATURE MODEL

FOR TARGET MATERIALS BOMBARDED BY ION BEAMS

I. INTRODUCTION

The ion implantation process can be broken into several steps. Initially, atoms of the desired alloy are ionized by stripping an electron from the outer shell. The mass of ions is then concentrated and accelerated by a variety of magnets and electric coils into a focussed beam. These accelerated ions then impinge upon the target material to form a thin alloyed layer in the substrate. The new surface usually shares some of the properties of both materials, but a synergism can also occur, resulting in a surface that is tougher or more corrosion resistant than its constituents.

This process lends itself to being very precise, controllable, and reproducible time after time. By controlling the energy of the ions, one controls the penetration of the ions into the substrate, and by varying the dose, the concentration of the alloy is determined.[1,2] Therefore, ion implanted profiles can be tailored to take advantage of specific material improvements at optimum depth and concentration values. Furthermore, the consistency enhances application towards high throughput processes such as bearings, circuit board drills, and other small manufactured items.

Substantial improvements by implanted dopants in the electrical, chemical, mechanical, or optical properties of many materials have prompted growth of research and applications of ion implantation. The advent of the computer stimulated groundwork for ion implantation

processes applicable to semiconductor fabrication, and now, research into ion implantation modification of manufacturing and industrial materials have opened new doors into materials research. Before the application of ion implantation to surface modification, the strict rules of metallurgy limited the number of compounds which could be mixed.[3] Poor coatings, or alloys, resulted from metals that simply would not dissolve into each other. The ability to introduce almost any element in the periodic table into the surface region of a material at low process temperatures, and in precisely controlled amounts provides an approach for surface modification with possibilities limited only by the imagination.[4] Elimination of conventional metallurgical constraints offers the potential to use a variety of alloying elements.

By the mid-1970s, applications to reduce wear and corrosion associated with metals and alloys had been investigated, and then confirmed in tools and components subjected to mild wear.[4,5] Since these preliminary investigations, the technology has expanded to address other problems in metallic workpieces, such as friction, fatigue, oxidation, and surface hardness. Improvements in these areas as a result of nitrogen implantation has made it the most heavily employed element. Several examples of lifetime improvements using nitrogen ion implantation are shown in Table 1.[3,6,7]

Life improvements have also been noted by using ion implantation on titanium based alloys (notably Ti-6Al-4V) used in orthopedic implants.[8,9] Additional research into alloys formed by the ion implantation process indicates other ions may significantly increase the lifetimes of various steels. Naval Research Laboratory programs have estimated life improvements in bearings made of AISI M50, 52100, or 440C

steels to be approximately a factor of 2.5 when the bearings are implanted with ions of chromium, molybdenum, boron, or a combination of these elements.[4] Still other researchers have shown improvements by implanting steels with titanium in the presence of carbon to form a metal carbide layer on the surface.[10,11]

Table 1
Improvements from Nitrogen Ion Implanting

Component	Material	Extends Life
Paper Slitters	Chrome-Steel	100%
Taps for Phenolic Resin	M2 Tool Steel	1000%
Thread Cutting Dies	M2 Tool Steel	400%
Slitters for Rubber	Tungsten Carbide	1000%
Wire Dies for Cu Wires	Tungsten Carbide	400%
Deep Drawing Dies	Tungsten Carbide	100%
Injection Molding Nozzle	Tool Steel	100%
Bearings	AISI 52100 Steel	100%
Mill Rolls	H-13 Steel	400%

On the other side of the coin, researchers have begun to look at ion beam processing in a novel way: to monitor wear rates. In this approach, small amounts of radioactive cobalt-60 are implanted a few angstroms into the walls of pipe. The amount of radiation in the fluid is monitored and then used to estimate the amount of wear in the pipe. Subsequently, if radiation levels have reached a pre-determined threshold, personnel will be alerted to the need for pipe replacement. This type of monitoring process is ideal for relatively inaccessible parts of chemical plants because it reduces the need for physical inspection.[3]

In addition to specific material improvements, acceleration in ion implantation technology has provided significant advances in developing models to understand and simulate corrosion, wear behavior, and

oxidation. Advances in understanding the mechanisms by which ion implantation modifies corrosion and wear behavior, along with an assessment of the constraints applicable to ion implantation, have helped to formulate guidelines on how and where implantation can be applied.[4] This information, in conjunction with design parameters defined by industry, can then be assimilated to develop prototype production facilities.

II. HEAT BUILD-UP DURING ION IMPLANTATION

Unlike other alloying techniques, ion implantation processes are conducted at relatively lower material temperatures. As it turns out, this lower temperature is both an advantage and a disadvantage. Most implantation is done at low temperatures to prevent thermal distortion and bulk property changes, and therefore it can be performed on finished pieces such as bearings or drill bits.[6,10] On the other hand, to achieve the high doses necessary for increased wear resistance, long exposure times and high fluences (>10^{17} ion/cm^2) of high energy ions (50-200 keV) can raise the target temperature from 25 to 1000 degrees Celsius.[10] As some research has noted, concern about the tribological properties of the material if there is a rapid rise in the surface and bulk temperature is an impetus to keep target materials at or near room temperature.[10,12] Since implantation takes place in a vacuum (no convective cooling) and radiation cooling has been shown to be inadequate for power densities of interest for large scale commercial operations, workstation materials must then act as an effective heat sink to prevent damage to target pieces and insure the quality of implantation.[14] Some machines incorporate cooling of the workpiece by contact conductance with a liquid cooled target holder, but this cooling can be a difficult engineering task considering the configuration of many workpieces: balls, wires, and other shapes.[4,6,12,13]

Consequently, the low temperature requirement for many applications limits the economic, and probably, physical success of the implantation. As noted previously, implantation is usually performed at lower ion energies over longer periods of time limiting throughput which

in turn drives up the cost.[5,10,12] Accordingly, much of the research directed towards improving the process (i.e., lowering the cost) has been devoted to developing adequate cooling of the target material. As one would expect, this cooling problem has been noted as a major design hurdle for a high throughput ion implantation facility.[4,14] Research also has been conducted to investigate improvements resulting from implantation with higher energy ions, as well as into targets with elevated temperatures.[6,12] Some have even speculated that ion implantation could permit a metallurgist to create new alloys by controlling the temperature of the solid during implantation so that ions could be implanted into crystal positions which would not form had the impurities been added at an earlier melt stage in the crystal growth.[6]

Research focussed on adequate target cooling for a high throughput ion implantation facility, or the modeling of high temperature implantation would be aided by a computer code that calculates the temperature distribution within a target material during implantation. The work explained here shows that a computer code developed to model plasma disruptions and subsequent energy deposition on a fusion reactor first wall can be used to adequately calculate surface and bulk temperature information during ion implantation. Therefore, researchers and production engineers could perform calculations to confirm the physical parameters necessary either to achieve the desired dose or to push the limits in investigating potential new alloys.

III. NUMERICAL SOLUTION OF THE PARTIAL DIFFERENTIAL EQUATION

During the implantation process a target material is bombarded by accelerated ions to form a thin alloyed layer in the substrate. As the ions suffer collisions with atoms in the target material they deposit their kinetic energy and thus raise the bulk temperature of the target material. The heat is then conducted to the target holder as long as there is a temperature gradient. A portion of the heat energy may be radiated to the surroundings. The geometry and thermophysical properties of the target and holder, as well as any active cooling of the holder will influence the conduction of the heat energy from the target. This physical process can be modeled with the general equation for transient heat conduction. The general equation for two-dimensional transient heat conduction in a cylindrical geometry is given as

$$pc\frac{dT}{dt} = \frac{1}{r}\frac{d}{dr}\left[kr\frac{dT}{dr}\right] + \frac{d}{dz}\left[k\frac{dT}{dz}\right] + q \qquad 3.1$$

where

$T(r,z,t) = T$ = temperature of the target material,
$p(T) = p$ = density of the target material,
$c(T) = c$ = specific heat of the target material,
$k(T) = k$ = thermal conductivity of the target material,
$q(t) = q$ = surface heat flux/radiative heat flux

and d denotes the partial differential operator.

The thermophysical material properties defined in equation 3.1 are temperature dependent. During the time step Δt, from n to n+1, the material properties will remain constant at values defined by the temperature profile at time equal to n. Prior to the next time step the properties will be recalculated using T_{n+1}. Hence, the equation can be written as,

$$\rho c \frac{dT}{dt} = \frac{kd}{rdr}\left[\frac{rdT}{dr}\right] + \frac{kd^2T}{dz^2} + q \qquad 3.2$$

Using the product rule of differentiation for the first term on the right hand side, the equation can be written as,

$$\rho c \frac{dT}{dt} = \frac{kdT}{rdr} + \frac{kd^2T}{dr^2} + \frac{kd^2T}{dz^2} + q \qquad 3.3$$

This can then be solved numerically utilizing the implicit Crank-Nicolson method in combination with an implicit alternating direction method over each time step, Δt.[15]

III.A. IMPLICIT CRANK-NICOLSON APPROXIMATIONS

The implicit Crank-Nicolson method starts with a Taylor's expansion approach of the partial derivatives which can be written as,

$$T(r+\Delta r, z+\Delta z, t+\Delta t) = T(r,z,t) + \left[\Delta x \frac{d}{dx} + \Delta z \frac{d}{dz} + \Delta t \frac{d}{dt}\right] T(r,z,t) +$$
$$\frac{1}{2!}\left[(\Delta x)^2 \frac{d^2}{dx^2} + (\Delta z)^2 \frac{d^2}{dz^2} + (\Delta t)^2 \frac{d^2}{dt^2}\right] T(r,z,t) + \ldots$$
$$\frac{1}{n!}\left[(\Delta x)^n \frac{d^n}{dx^n} + (\Delta z)^n \frac{d^n}{dz^n} + (\Delta t)^n \frac{d^n}{dt^n}\right] T(r,z,t) \qquad 3.4$$

Then the forward and backward difference equations for dT/dt at the halfway point of a time step (i.e., $\Delta t/2$) can be written as,

$$T_{i,j,n+1} = T_{i,j,n+1/2} + \frac{\Delta t}{2} T_t + \frac{\Delta t^2}{4} T_{tt} + \frac{\Delta t^3}{12} T_{ttt} + \ldots \text{(forward)} \qquad 3.5$$

$$T_{i,j,n} = T_{i,j,n+1/2} - \frac{\Delta t}{2} T_t + \frac{\Delta t^2}{4} T_{tt} - \frac{\Delta t^3}{12} T_{ttt} + \ldots \text{(backward)} \qquad 3.6$$

and by subtracting the backward difference equation from the forward difference equation the resulting equation will be given as,

$$T_{i,j,n+1} - T_{i,j,n} = \Delta t\ T_t + \frac{\Delta t^3}{6} T_{ttt} + \ldots \qquad 3.7$$

and,

$$T_t = \frac{dT}{dt} = \frac{T_{i,j,n+1} - T_{i,j,n}}{\Delta t} + R\{(\Delta t)^3\} \qquad 3.8$$

where $R\{(\Delta t)^3\}$ is the remainder which is on the order of $(\Delta t)^3$.

Similarly the forward and backward difference equations in the radial direction can be written at the same halfway point as,

$$T_{i+1,j,n+1/2} = T_{i,j,n+1/2} + \Delta r\ T_r + \frac{\Delta r^2}{2!} T_{rr} + \frac{\Delta r^3}{3!} T_{rrr} + \ldots \text{(forward)} \qquad 3.9$$

and,

$$T_{i-1,j,n+1/2} = T_{i,j,n+1/2} - \Delta r\ T_r + \frac{\Delta r^2}{2!} T_{rr} - \frac{\Delta r^3}{3!} T_{rrr} + \ldots \text{(backward)} \qquad 3.10$$

Adding equations 3.5 and 3.6 gives,

$$T_{i,j,n+1/2} = \frac{T_{i,j,n+1} + T_{i,j,n}}{2} + R\{(\Delta t)^2\} \qquad 3.11$$

then substituting this relationship into equations 3.9 and 3.10 yields,

$$\frac{T_{i+1,j,n+1} + T_{i+1,j,n}}{2} = \frac{T_{i,j,n+1} + T_{i,j,n}}{2} + \Delta r\ T_r + \frac{\Delta r^2}{2!} T_{rr} + \frac{\Delta r^3}{3!} T_{rrr} + R\{(\Delta t)^2\} + R\{(\Delta r)^4\} \qquad 3.12$$

$$\frac{T_{i-1,j,n+1} + T_{i-1,j,n}}{2} = \frac{T_{i,j,n+1} + T_{i,j,n}}{2} - \Delta r\ T_r + \frac{\Delta r^2}{2!} T_{rr} - \frac{\Delta r^3}{3!} T_{rrr} + R\{(\Delta t)^2\} + R\{(\Delta r)^4\} \qquad 3.13$$

Now adding equations 3.12 and 3.13 yields,

$$T_{i+1,j,n+1} + T_{i+1,j,n} + T_{i-1,j,n+1} + T_{i-1,j,n} = 2T_{i,j,n+1} + 2T_{i,j,n} + 2(\Delta r)^2\ T_{rr} + R\{(\Delta t)^2\} + R\{(\Delta r)^4\} \qquad 3.14$$

which results in a finite difference approximation for the second order partial derivative in the radial direction. This is written as,

$$T_{rr} = \frac{T_{i-1,j,n+1} - 2T_{i,j,n+1} + T_{i+1,j,n+1}}{2(\Delta r)^2} + \frac{T_{i-1,j,n} - 2T_{i,j,n} + T_{i+1,j,n}}{2(\Delta r)^2} + R\{(\Delta t)^2\} + R\{(\Delta r)^4\} \quad 3.15$$

$$= 1/2D_r^2\, T_{i,j,n+1} + 1/2D_r^2\, T_{i,j,n} + R\{(\Delta t)^2\} + R\{(\Delta r)^4\}$$

where D_r denotes the central difference operator with respect to r.[15]

The same Taylor's expansion method can be used to write the Crank-Nicolson form of the finite difference equation for the second order partial derivative in the axial direction as,

$$T_{zz} = \frac{T_{i,j-1,n+1} - 2T_{i,j,n+1} + T_{i,j+1,n+1}}{2(\Delta z)^2} + \frac{T_{i,j-1,n} - 2T_{i,j,n} + T_{i,j+1,n}}{2(\Delta z)^2} + R\{(\Delta t)^2)\} + R\{(\Delta z)^4\} \quad 3.16$$

$$= 1/2D_z^2\, T_{i,j,n+1} + 1/2D_z^2\, T_{i,j,n} + R\{(\Delta t)^2\} + R\{(\Delta z)^4\}$$

The first order partial differential in the radial direction is approximated by a finite difference equation similar to that of the time derivative. By subtracting equation 3.13 from equation 3.12,

$$T_{i+1,j,n+1} + T_{i+1,j,n} - T_{i-1,j,n+1} - T_{i-1,j,n} = 4\Delta r\, T_r + R\{(\Delta t)^2\} + R\{(\Delta r)^3\}$$

and so,

$$T_r = \frac{T_{i+1,j,n+1} - T_{i-1,j,n+1} + T_{i+1,j,n} - T_{i-1,j,n}}{4\Delta r} + R\{(\Delta t)^2\} + R\{(\Delta r)^3\} \quad 3.17$$

$$= 1/2D_r\, T_{i,j,n+1} + 1/2D_r\, T_{i,j,n} + R\{(\Delta t)^2\} + R\{(\Delta r)^3\}$$

Now equations 3.8, 3.15, 3.16, and 3.17 can be used to write a finite difference approximation for equation 3.3.

$$\rho c\left[\frac{T_{i,j,n+1} - T_{i,j,n}}{\Delta t}\right] =$$
$$\frac{k}{i\Delta r}\left[\frac{T_{i+1,j,n+1} - T_{i-1,j,n+1}}{4\Delta r} + \frac{T_{i+1,j,n} - T_{i-1,j,n}}{4\Delta r}\right] +$$
$$k\left[\frac{T_{i-1,j,n+1} - 2T_{i,j,n+1} + T_{i+1,j,n+1}}{2(\Delta r)^2} + \frac{T_{i-1,j,n} - 2T_{i,j,n} + T_{i+1,j,n}}{2(\Delta r)^2}\right] +$$
$$k\left[\frac{T_{i,j-1,n+1} - 2T_{i,j,n+1} + T_{i,j+1,n+1}}{2(\Delta z)^2} + \frac{T_{i,j-1,n} - 2T_{i,j,n} + T_{i,j+1,n}}{2(\Delta z)^2}\right] +$$
$$q + R\{(\Delta t)^2 + (\Delta r)^3 + (\Delta z)^4\}$$

Then rearranging and combining like terms yields,

$$\left[\frac{k}{4i(\Delta r)^2} - \frac{k}{2(\Delta r)^2}\right]T_{i-1,j,n+1} + \left[\frac{k}{(\Delta r)^2} + \frac{k}{(\Delta z)^2} + \frac{\rho c}{\Delta t}\right]T_{i,j,n+1} +$$
$$\left[\frac{-k}{4i(\Delta r)^2} - \frac{k}{2(\Delta r)^2}\right]T_{i+1,j,n+1} + \left[\frac{-k}{2(\Delta z)^2}\right]T_{i,j-1,n+1} + \left[\frac{-k}{2(\Delta z)^2}\right]T_{i,j+1,n+1} =$$
$$\left[\frac{-k}{4i(\Delta r)^2} + \frac{k}{2(\Delta r)^2}\right]T_{i-1,j,n} + \left[\frac{\rho c}{\Delta t} - \frac{k}{(\Delta r)^2} - \frac{k}{(\Delta z)^2}\right]T_{i,j,n} +$$
$$\left[\frac{k}{4i(\Delta r)^2} + \frac{k}{2(\Delta r)^2}\right]T_{i+1,j,n} + \left[\frac{k}{2(\Delta z)^2}\right]T_{i,j-1,n} + \left[\frac{k}{2(\Delta z)^2}\right]T_{i,j+1,n} +$$
$$q + R\{(\Delta t)^2 + (\Delta r)^3 + (\Delta z)^4\}$$

or, more simply as,

$$AT_{i-1,j,n+1} + BT_{i,j,n+1} + CT_{i+1,j,n+1} + DT_{i,j-1,n+1} + ET_{i,j+1,n+1} = T \qquad 3.18$$

where,

$$A = \frac{k}{2(\Delta r)^2}\left[\frac{1}{2i} - 1\right]$$

$$B = \frac{k}{(\Delta r)^2} + \frac{k}{(\Delta z)^2} + \frac{\rho c}{\Delta t}$$

$$C = \frac{k}{2(\Delta r)^2}\left[\frac{-1}{2i} - 1\right]$$

$$D = \frac{-k}{2(\Delta z)^2}$$

$$E = \frac{-k}{2(\Delta z)^2}$$

and,

$$T = -AT_{i-1,j,n} + \left[\frac{pc}{\Delta t} - \frac{k}{(\Delta r)^2} - \frac{k}{(\Delta z)^2}\right]T_{i,j,n} - CT_{i+1,j,n} -$$

$$DT_{i,j-1,n} - ET_{i,j+1,n} + q$$

Equation 3.18 shows that the resulting system of linear equations will have five unknowns per equation: $T_{i-1,j,n+1}$, $T_{i,j,n+1}$, $T_{i+1,j,n+1}$, $T_{i,j-1,n+1}$ and $T_{i,j+1,n+1}$. This is a disadvantage since the system is not tridiagonal and would require a considerable amount of computation utilizing a Gaussian elimination scheme. To avoid this expense, an implicit alternating direction method, as discussed by Peaceman and Rachford, can be employed to develop successive tridiagonal matrices over the time step, Δt, instead of the one matrix defined by equation 3.18.[15] The method halves the time step, Δt, and then for the first half of the time step (t/2), equation 3.18 is only implicit in the radial direction, and then for the second part of the time step equation 3.18 is implicit in the z-direction only. Using the notation defined previously, in a simplified form, the two steps are given as,

$$AT_{i-1,j}^{*} + B'T_{i,j}^{*} + CT_{i+1,j}^{*} = T' \qquad 3.19$$

where,

$$B' = \frac{pc}{\Delta t^{*}} + \frac{k}{(\Delta r)^2}$$

$$T' = -AT_{i-1,j,n} + \left[\frac{pc}{\Delta t^{*}} - \frac{k}{(\Delta r)^2} - \frac{2k}{(\Delta z)^2}\right]T_{i,j,n} - CT_{i+1,j,n} - 2DT_{i,j,n}$$

$$- 2ET_{i,j+1,n} + q$$

and

$$B''T_{i,j,n+1} + DT_{i,j-1,n+1} + ET_{i,j+1,n+1} = T'' \quad 3.20$$

where,

$$B'' = \frac{pc}{\Delta t^*} + \frac{k}{(\Delta z)^2}$$

$$T'' = -2AT_{i-1,j}^* + \left[\frac{pc}{\Delta t^*} - \frac{2k}{(\Delta r)^2} - \frac{k}{(\Delta z)^2}\right]T_{i,j}^* - 2CT_{i+1,j}^* - DT_{i,j-1}^*$$

$$-ET_{i,j+1}^* + q$$

where $T_{i,j}^*$ denotes the temperature at node i,j after the solution at $\Delta t/2$.

Equations 3.19 and 3.20 are used to develop a tridiagonal system for nodes i=2 to i=rmax-2 and j=2 to j=zmax-2, where rmax and zmax are the radius and thickness of the target material respectively. The linear equations for i=1 and i=rmax-1 and j=1 and j=zmax-1 will be defined by the boundary conditions outlined in the following sections.

III.B. Initial Condition

The initial condition simply defines the temperature distribution within the target prior to ion beam interaction: $T(r,z,0) = T_{amb}$. For the examples shown in this paper the initial temperature distribution has been constant throughout the sample, either at room temperature or some preheat temperature.

III.C. Boundary Conditions

The four boundary conditions for the model are depicted in Figure 1. The temperature of the target at its maximum radius, rmax,

Figure 1. Depiction of Boundary Conditions

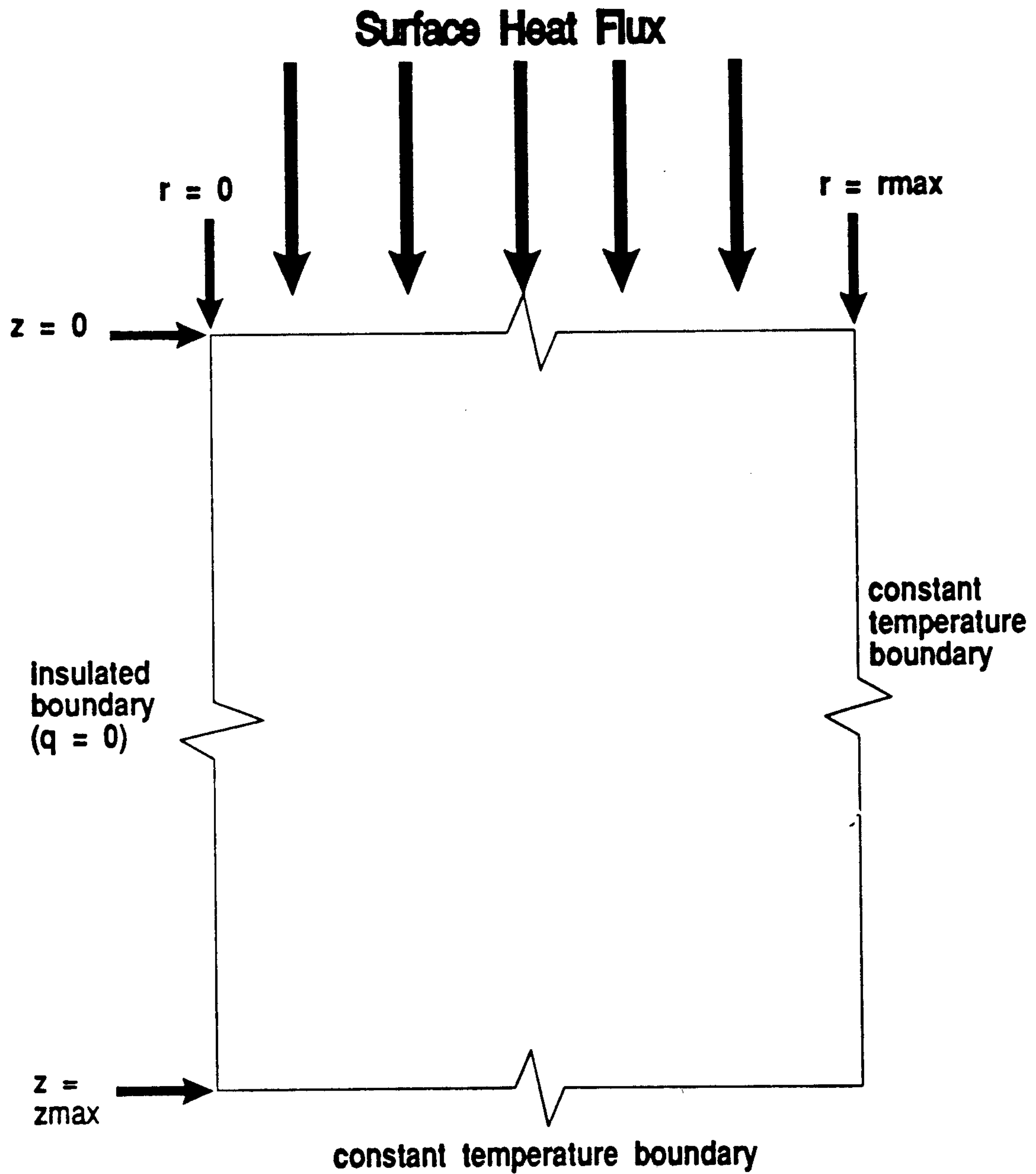

and maximum depth, zmax, are held constant throughout the calculation, which corresponds to a target holder that is continuously cooled. Therefore, for the first half of the time step equation 3.19 can be written as,

$$AT_{rmax-2,j}^{*} + B'T_{rmax-1,j}^{*} = -CT_{rmax,j} + T' \quad 3.21$$

for j=2 to zmax-1.

For the second half of the time step, equation 3.20 is written as,

$$DT_{i,zmax-2,n+1} + B''T_{i,zmax-1,n+1} = -ET_{i,zmax,n+1} + T'' \quad 3.22$$

for i=2 to rmax-1.

The centerline of the target (i=1) is treated as an insulated boundary, and therefore no heat transfer takes place, or,

$$\left.\frac{dT}{dr}\right|_{r=0} = 0 \quad 3.23$$

To define a finite difference approximation of the first order partial derivative at the centerline of the target, consider a "pseudo node" on the other side of the centerline as in Figure 2.[16] If the partial first order derivative with respect to r is then approximated by,

$$\frac{dT}{dr} = 0 = \frac{T_0 - T_2}{2\Delta r} \quad 3.24$$

then

$$T_0 = T_2 \quad 3.25$$

Figure 2. Insulated Boundary Condition

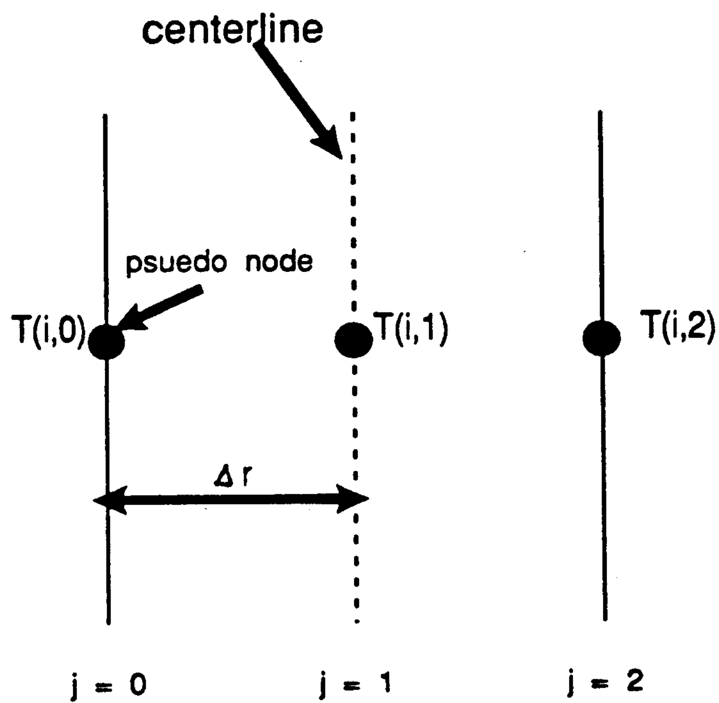

Figure 3. Surface Condition

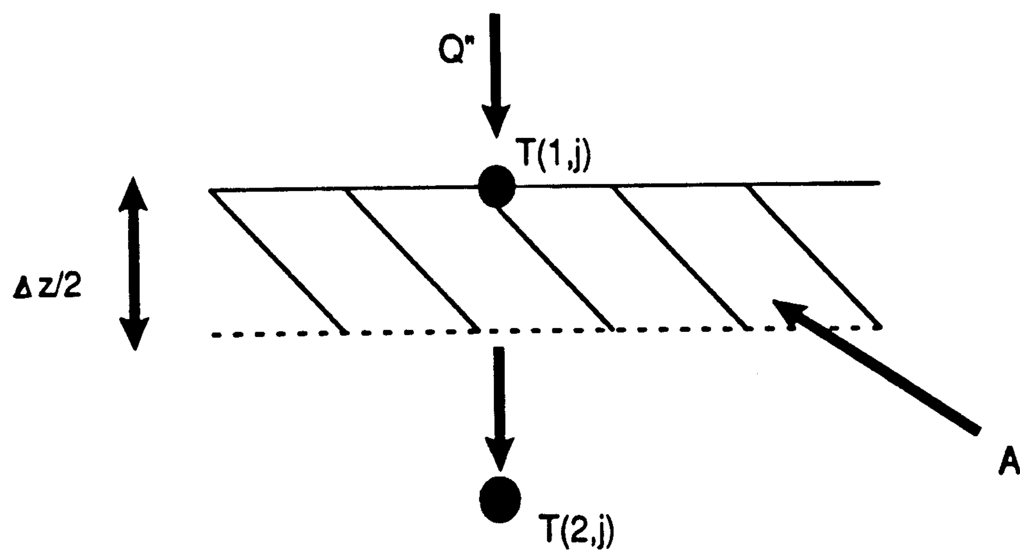

Now incorporating this relationship into equation 3.19, the first equation in the radially implicit tridiagonal matrix is,

$$B'T_{i,j}^{*} + (A+C)T_{i+1,j}^{*} = T' \qquad 3.26$$

The final boundary condition needed is the surface heat flux which is dependent on the energy density (J/cm^2), the radius of the incident beam (cm), and the deposition time (seconds). There will be a value of heat flux for nodes at the surface within the radius of the incident beam until deposition is complete. After the deposition time has been completed, the boundary condition will be defined by a radiative boundary condition.

From Figure 3, and knowing that the heat into a volume minus the heat out of the volume is equal to the energy stored in the volume, the boundary condition is written as

$$q''A + kA\left.\frac{dT}{dz}\right|_{z=\frac{\Delta z}{2}} = \frac{pc\ A\Delta z}{2}\frac{dT}{dt} \qquad 3.27$$

Next, eliminating A and using approximations for the first order partial derivatives, this equation can be written as,

$$q'' + k\left[\frac{T_{i,2,n+1} - T_{i,1,n+1}}{\Delta z}\right] = \frac{pc\Delta z}{2}\left[\frac{T_{i,1,n+1} - T_{i,1,n}}{\Delta t}\right] \qquad 3.28$$

and combining like terms,

$$\left[\frac{k}{\Delta z} + \frac{pc\Delta z}{2\Delta t}\right]T_{i,1,n+1} - \frac{k}{\Delta z}T_{i,2,n+1} = \frac{pc\Delta z}{2}T_{i,1,n} + q'' \qquad 3.29$$

During the deposition q" is the surface heat flux in $J/sec\text{-}cm^2$, and after the deposition is finished it is a radiative heat transfer value dependent on T_1 and T_{amb}.

IV. ATHERMAL*2

Calculation of the temperature distribution in a target material during ion implantation was accomplished using the ATHERMAL*2 computer code.[17] Dr. Ahmed Hassanein, with Argonne National Laboratory, developed the code to model accurately experiments in which ion or electron beams are used to simulate plasma disruption in fusion reactors. Impetus for this research stems from interest in determining the exact amount of vaporization losses and melt layer thickness resulting from a plasma disruption. These parameters are in turn important in determining fusion reactor design and lifetime.[18]

ATHERMAL*2 was developed to provide a theoretical model of an ion or electron beam experiment so that the effects of lateral heat conduction and beam spatial distribution during the experiment could be considered. To provide the necessary flexibility, the code solves the two-dimensional heat conduction equation in cylindrical coordinates with moving boundaries. Inclusion of a moving boundaries for the melt-solid interface or the surface receding as a result of evaporation from the surface is not necessary for the scope of this work. After all, the main objective during ion implantation is to keep target materials well below their melting temperature to prevent deformation (explanation of the moving boundary model can be found in references 18,19,20, and 21). The employment, however, of this algorithm would be useful to determine the onset of melting and the associated damage if too much energy is delivered to a target. Additionally, in the future there may be some applications where melting is useful to modify the surface

characteristics. For example, the combination of introducing impurity ions to the surface layer with re-crystalization might be useful.

IV.A INPUT PARAMETERS

To simplify the model, the heat source term is assumed to be a surface heat flux. This approximation is adequate given that implanted ions only penetrate on the order of microns into the surface of the target material, and thus the energy of the ion is deposited in this range.[17,19,20] The input to ATHERMAL*2 for the surface heat flux is in the form of an energy density, J/cm^2.

Other input parameters include the radius of the target material (cm), radius of the beam (cm), ambient temperature of the target (deg Kelvin), temperature of the medium where the sample is irradiated (deg Kelvin), and the choice of material for the target. Most of the materials (such as vanadium, tantalum, molybdenum, etc.) included in the subroutine devoted to calculating the temperature dependent thermophysical properties of the target are those considered for future applications in fusion reactors. In addition, aluminum, copper, and stainless steel (materials that have been ion implantation target materials) are included as well.

IV.B SURFACE HEAT FLUX

The total energy deposited onto the surface of the target material is then calculated based upon the energy distribution within the beam (known as the beam shape). ATHERMAL*2 has the capability to handle both

flat and Gaussian shaped beams (see Figure 4). If F_f denotes the energy density for a flat beam, then the total energy of the beam is simply,

$$P_f = F_f \pi r_b^2 \quad 4.1$$

where r_b denotes the nominal radius of the beam.

Now, if F_G denotes the maximum heat flux at the center of the Gaussian beam, then,

$$F(r) = F_G(\exp(-r^2/2\mathrm{sigma}^2)) \quad 4.2$$

defines the surface heat flux profile along the radius of the beam. The standard deviation, sigma, can be calculated by noting that at the nominal beam spot radius $r = r_b$, the local heat flux is one half the maximum, F_G. Therefore,

$$1/2F_G = F_G(\exp(-r_b^2/2\mathrm{sigma}^2)) \quad 4.3$$

and

$$1/2 = \exp(-r_b^2/2\mathrm{sigma}^2) \quad 4.4$$

Then taking the natural logarithm of both sides,

$$\ln(1/2) = -r_b^2/2\mathrm{sigma}^2 \quad 4.5$$

or,

$$2\mathrm{sigma}^2 = -r_b^2/\ln(1/2) \quad 4.6$$

and finally,

$$\mathrm{sigma}^2 = 0.721 r_b^2 \quad 4.7$$

Figure 4. Schematic Illustrating Ion Beam - Target Interaction

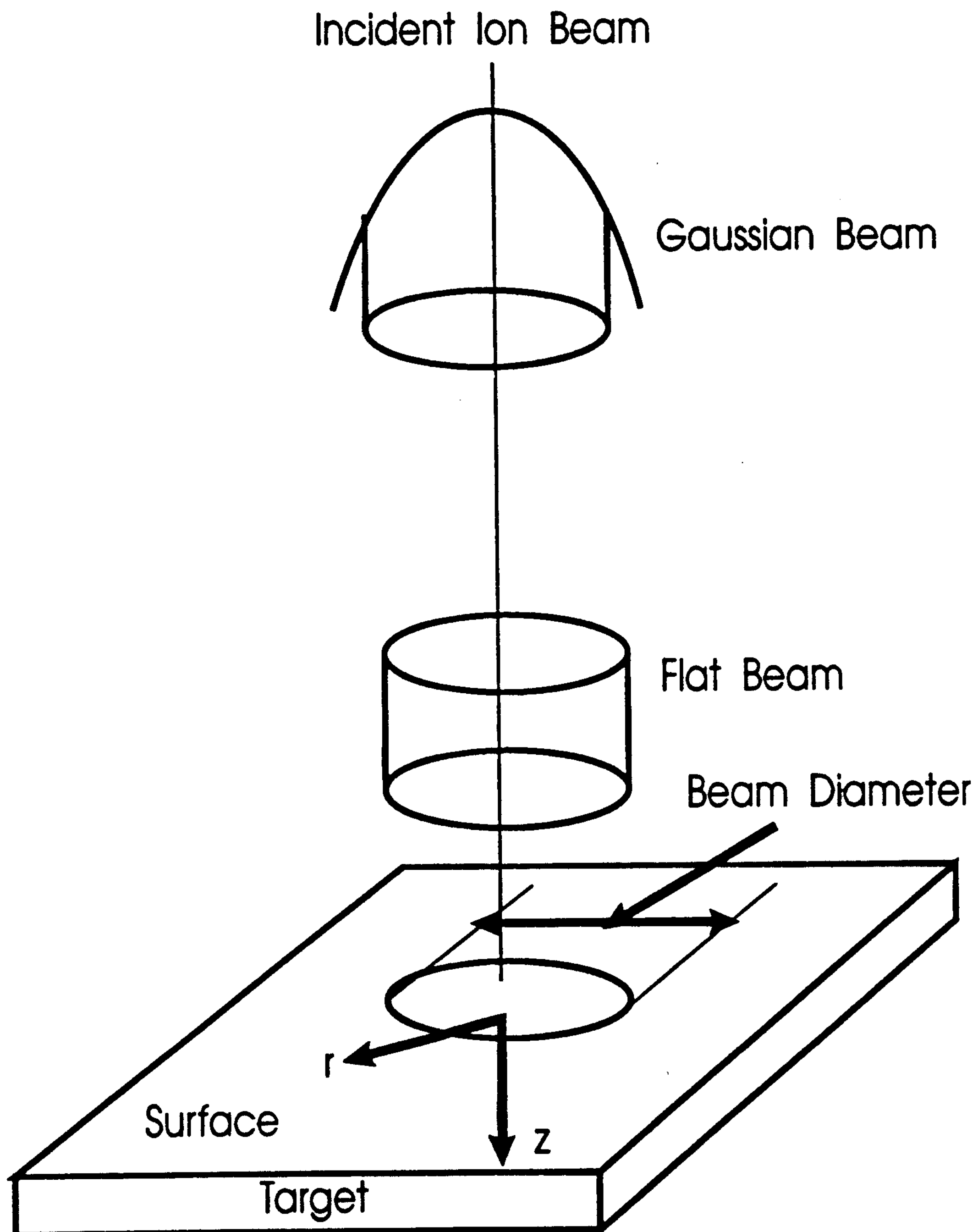

The total power for the Gaussian profile is calculated by integrating the surface heat flux profile over the circular area of the beam. Thus,

$$P_G = \int_0^\infty F_G(\exp(-r^2/2sigma^2))\ 2\pi r dr \qquad 4.8$$

$$= F_G 2\pi \int_0^\infty \exp(-r^2/2sigma^2)\ rdr$$

$$= F_G 2\pi \{\exp(-r^2/2sigma^2) * sigma^2 \Big|_0^\infty \}$$

$$= F_G 2\pi\ sigma^2$$

From an experimental point of view, the total energy of the beam is known more precisely than the beam profile itself. Subsequently if,

$$P_{tot} = P_f = P_G \qquad 4.9$$

then

$$F_f \pi r_b^2 = F_G 2\pi\ sigma^2 \qquad 4.10$$

By solving for F_G we see that

$$F_G = 1/2(r_b^2/sigma^2)F_f \qquad 4.11$$

and remembering that $sigma^2 = 0.721r_b^2$,

$$F_G = 0.694F_f \qquad 4.12$$

Therefore, the maximum heat flux of the Gaussian profile is less than the maximum heat flux of the flat beam profile. This implies that given the same total beam energy, a flat beam distribution will translate into a larger surface heat flux, and consequently a higher surface temperature compared to a Gaussian beam distribution.[18] All calculations outlined in the next section assume a flat beam profile

since this would define the limiting case (i.e., largest surface heat flux for a given total beam energy).

The value of the ion beam energy density (J/cm^2) can be calculated several ways depending upon what parameters are used to characterize the beam. First, if the beam is characterized by an ion flux ($ions/cm^2$-sec) and the energy of the individual ions (eV), then the energy density is simply the product of the flux, energy, and a conversion factor for eV to joules.[17,22] Secondly, the ion beam may be defined by a beam current and the voltage through which the ions have been accelerated. The beam energy density is then the product of the beam current (A) and the voltage (V); a conversion factor is not necessary.[17,22]

V. CALCULATIONS

This paper presents a model of the Sampath and Wilbur experiment outlined in their article "Broad Beam Ultrahigh Current Density Ion Implantation" using ATHERMAL*2.[12] Specifically, this model considered the implantation of nitrogen ions into stainless steel because the other materials investigated by Sampath and Wilbur are not included in the available version of ATHERMAL*2.

V.A. THE SAMPATH AND WILBUR EXPERIMENT

The experimental apparatus consisted of an ion source, an accelerator plate, a graphite mask/shutter, and a water-cooled sample holder all contained in a vacuum chamber (refer to Figure 5 for a depiction of the implantation system). In short, positively charged ions from the source are accelerated, proportional to the voltage of the accelerator plate, towards the target material. The movable graphite assembly near the sample holder masks all samples except the one being implanted. Finally, the sample holder itself is water-cooled to assure that the samples were at the cooling water temperature prior to the initiation of ion implantation, to provide a constant heat sink, and to facilitate rapid cooling of the sample once the implantation is complete. More detail about the sample holder is provided in the next section since it is important in defining various input parameters to the code (namely the radius of the beam, radius of the sample, initial temperatures, etc.), and additional detail about the remainder of the apparatus can be found in reference 12.

Figure 5. Schematic of Implantation System

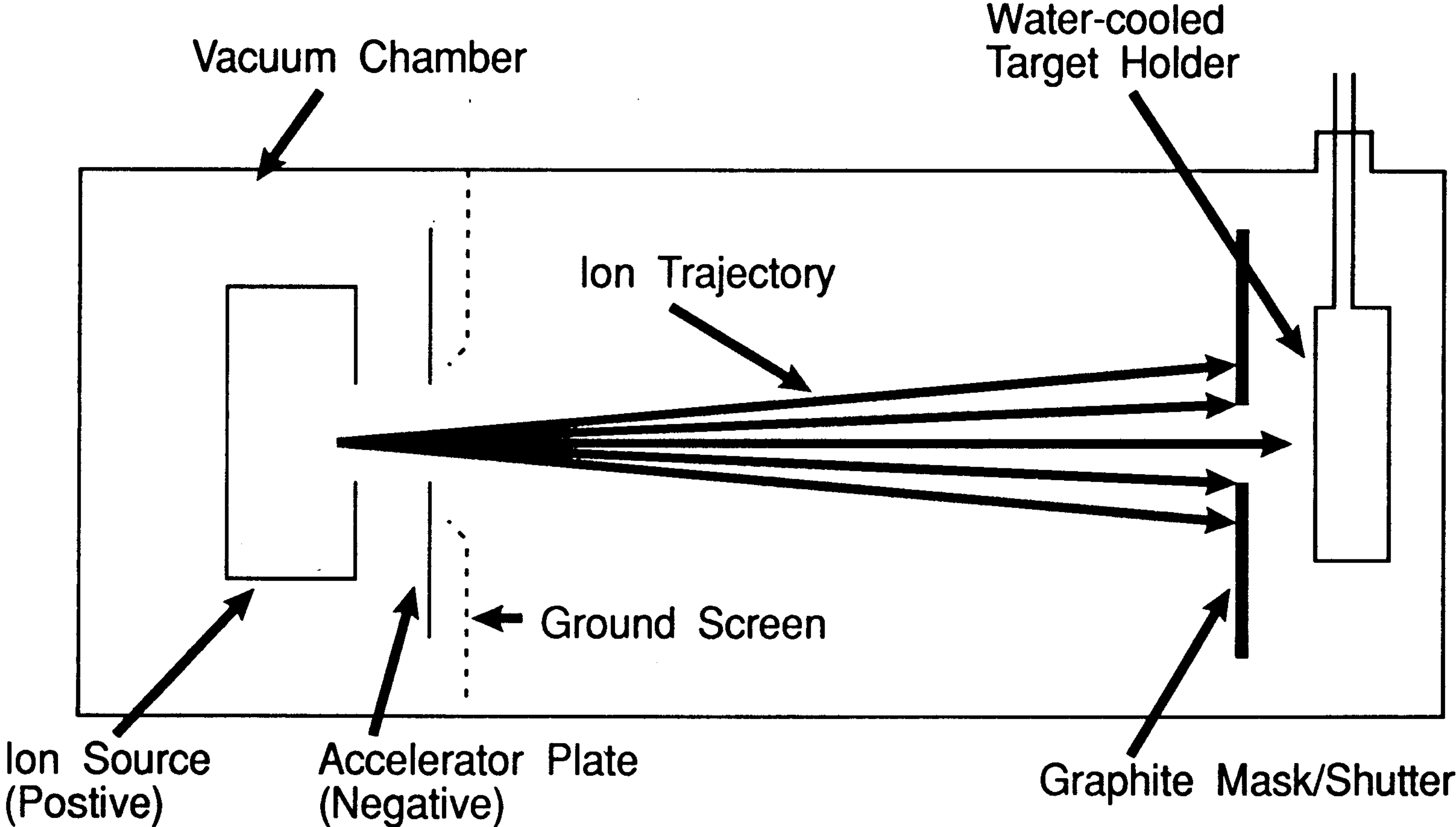

V.B. MODELING APPROXIMATIONS

Figure 6 depicts the details of the water-cooled sample holder. The target "blocks" are 0.5cm wide by 1.6cm high by 1.0cm thick and imbedded in a copper heat sink that is convectively cooled by water. Note that in the "straight-on" view the graphite mask shutter is not shown whereas in the "side" view it is. In the "straight-on" view the clear area denotes the implantation area versus the masked regions, which are denoted by the shaded areas. For adaptation to modeling with the two-dimensional computer code the geometry pictured in Figure 6 must be translated into a cylindrical approximation. Since the thermal conductivity of copper is much greater than that of stainless steel, the heat transfer from the target "block" being implanted would be lowest at the sides adjacent to the other stainless steel blocks which are only separated by a thin copper sheet. Thus, a conservative approximation to the real target geometry would be three target "blocks" oriented side by side as shown in Figure 7. In this depiction the cross-hatched area represents the implanted surface area. The total surface area of the stainless steel is then (3 x 0.5cm) x 1.6cm = $2.40cm^2$, and the implanted surface area is 0.5cm x 1.6cm = $0.80cm^2$. Subsequently, if r_{max} denotes the radius of a circular stainless steel target with the same total surface area as the three "blocks" oriented side by side then,

$$\pi r_{max}^2 = 2.40cm^2 \qquad 5.1$$

and

$$r_{max} = 0.87cm \qquad 5.2$$

Figure 6. Target Holder to be Modeled

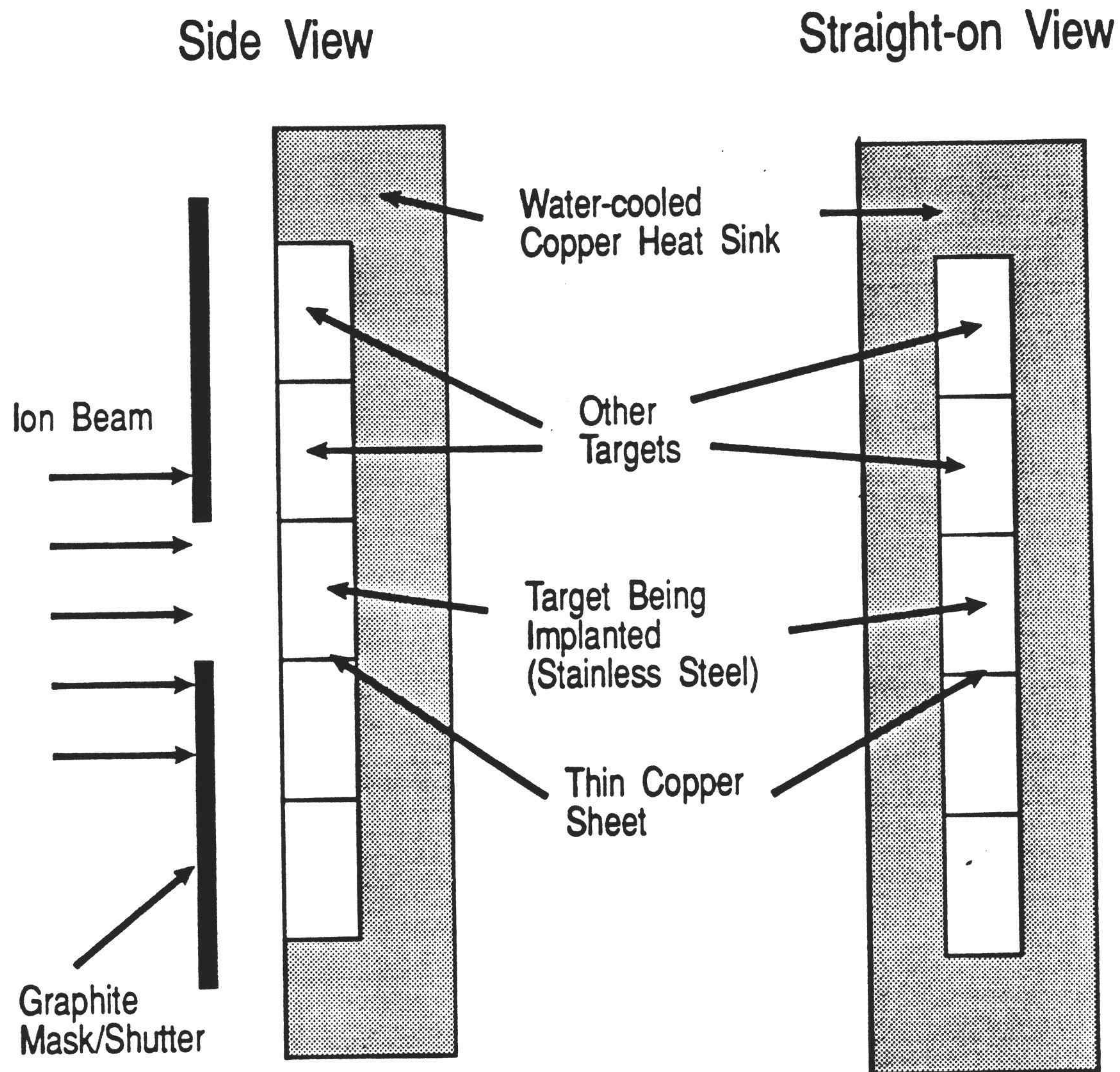

Figure 7. Cylindrical Geometry Approximation for Target Holder

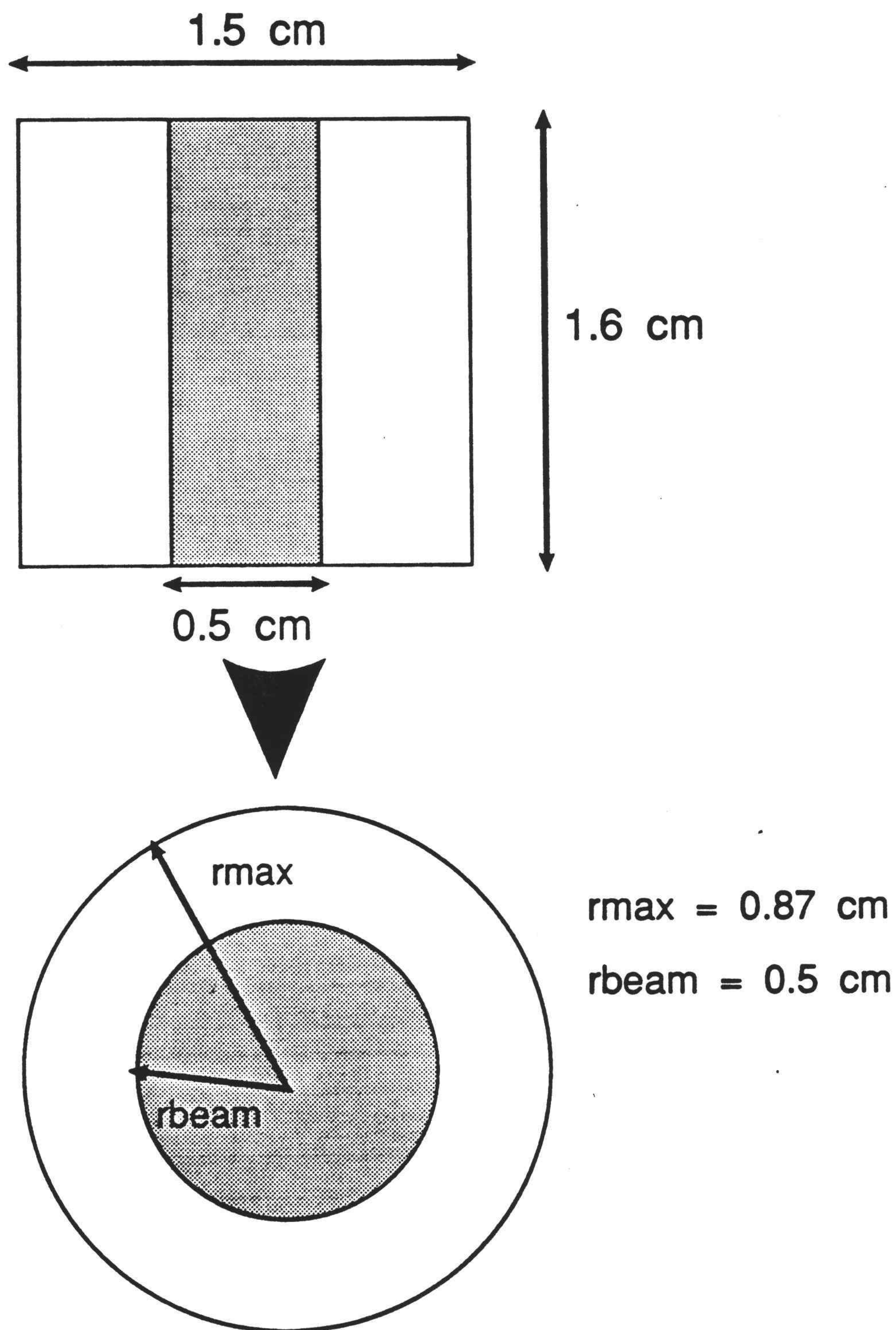

Likewise, if r_{beam} denotes the radius of the beam, which is turn defines the radius of the implanted surface area in a cylindrical geometry then,

$$\pi r_{beam}^2 = 0.80cm^2 \quad 5.3$$

and

$$r_{beam} = 0.50cm \quad 5.4$$

In ATHERMAL*2 the distance between the radial nodes is calculated by dividing the value of r_{max}, the target radius, by 48. For ease of reading the output and to retain an adequate number of significant figures because of the output format, r_{max} was taken to be 0.96cm.

V.C. SOURCE INPUT

In their article, Sampath and Wilbur illustrate the affect of high current density implantation versus low current density implantation on the surface temperature. This paper concentrates only on the high current density example, and therefore an energy density for this case is needed. All of the parameters mentioned in Section IV needed to determine the energy density of the incident ion beam are provided in the Sampath and Wilbur article; namely, energy of the ions, a total dose, the current density, and the total deposition time. It is important to note that the targets were implanted so that the total dose was "greater than or equal to 1×10^{17} N_2^+ions/cm^2." The assumption here will be that a total dose of 1×10^{17} ions/cm^2 was implanted into the stainless steel target in 11.0 seconds. This translates into a dose rate of 9.1×10^{15} ions/cm^2-sec at the high current density of

$1500 uA/cm^2$. This dose rate will become important in considering a second case later in which only the total dose and current density are listed.

As before, the energy density can be calculated in two different ways. For the first method the total dose is simply multiplied by the ion energy and a conversion factor,

$$E = (1x10^{17} ions/cm^2)(60x10^3 eV/ion)(1.60219x10^{-19} J/ev) \quad 5.5$$
$$= 961\ J/cm^2$$

The second method is to multiply the ion beam current density, the accelerating voltage (same as the ion energy), and the deposition time,

$$E = (1500 uA/cm^2)(60x10^3 V)(11.0 sec) \quad 5.6$$
$$= 990\ J/cm^2$$

The 3% difference in the two methods is not significant and is attributable to the uncertainty in the value of the total dose. The second method is used because it is independent of the total dose and thus more accurate, and because it is a higher energy density which would result in a greater rise in the surface temperature.

The other input parameters include the ambient temperature of the target material (12 deg Celsius), and of course the type of material used as a target; stainless steel.[12]

V.D. RESULTS

Three separate models were run to compare the centerline surface temperature profile for one- and two-dimensional calculations, as well

as to show the effect of varying the ion beam radius (i.e., the amount of exposed surface). The one-dimensional values were calculated using a short program supplied by Dr. Alan H. Robinson and modified to model stainless steel.[23] The one-dimensional program used an implicit finite difference method to generate a system of linear equations which were then solved using a Gaussian elimination scheme. Development of the one-dimensional implicit finite difference equations for this program and the treatment of the initial and boundary conditions is very much the same as the methods presented earlier for the two-dimensional scheme. The one-dimensional code is different in that the material properties (density, heat capacity, and thermal conductivity) remain at constant values throughout the entirety of the program.

It should be noted that there was some difficulty with the input values for the surface heat flux in ATHERMAL*2. The author of this paper had no access to the code to attempt correction of this problem, therefore the source input values were chosen such that the maximum surface temperature calculated for the two-dimensional solution corresponded closely with the maximum surface temperature measured, and reportedly calculated using a one-dimensional model, by Sampath and Wilbur (i.e., approximately 450 deg Celsius).[12] Although this approach prejudices any comparison of the merits of a one-dimensional calculation and the two-dimensional calculation, it is still relevant to discussing the potential application of the code for analysis of beam target interaction. Furthermore, it points out that the ATHERMAL*2 code could be modified if there was interest by someone to do so in the future.

Figure 8 shows the centerline surface temperature profile for the one-dimensional calculation and a two-dimensional calculation with a

Figure 8. Centerline Surface Temperature (11 sec deposition)

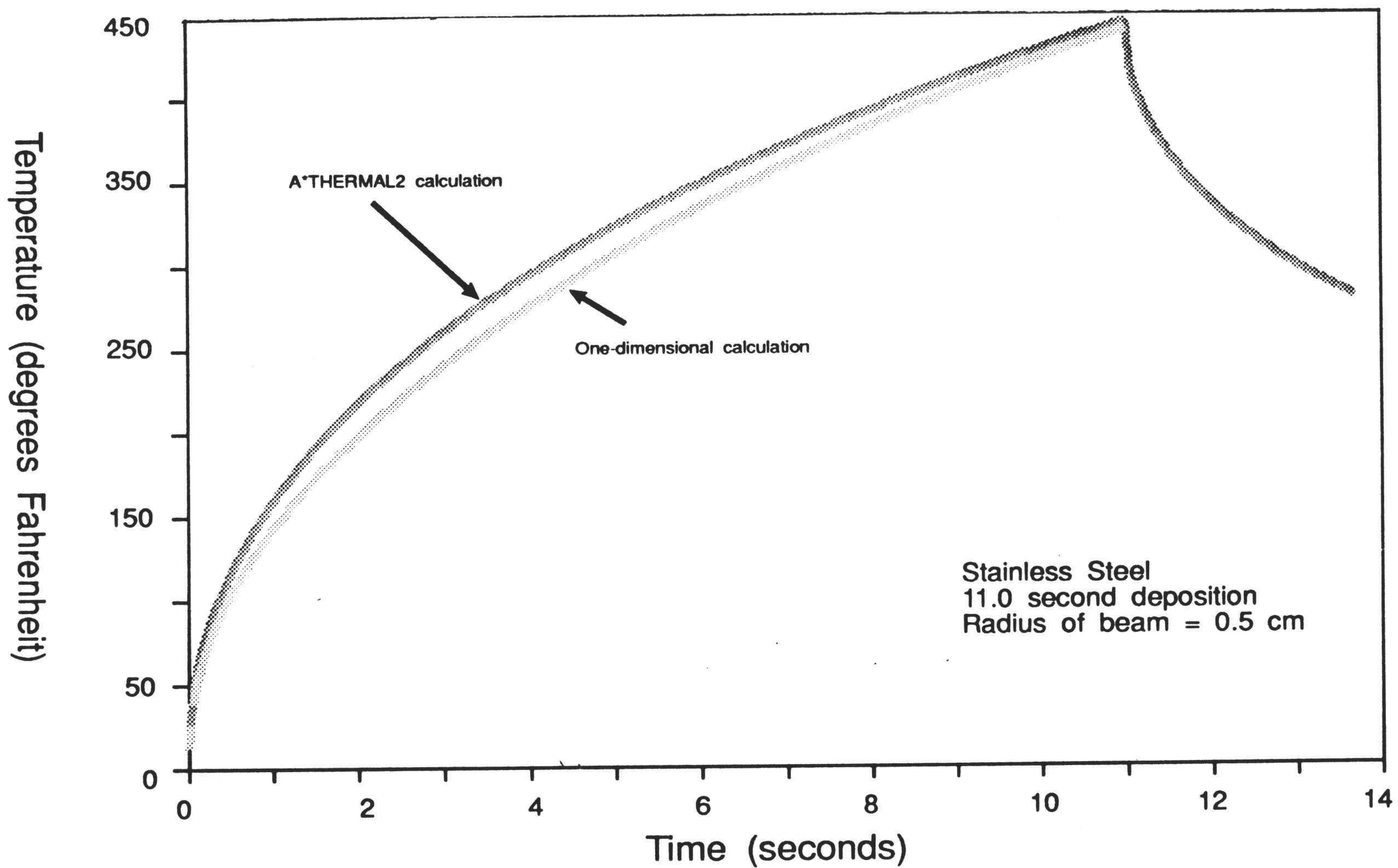

0.5cm radius beam. The maximum centerline surface temperature for the two-dimensional calculation was 446 deg Celsius and for the one-dimensional calculation it was 441 deg Celsius. Two other two-dimensional calculations with beam radii of 0.48cm and 0.52cm produced maximum centerline surface temperatures of 444 deg Celsius and 447 deg Celsius respectively. The consistency of the ATHERMAL*2 results with Sampath and Wilbur's measured and calculated maximum surface temperature, in conjunction with the agreement of the time-dependent behavior with the one-dimensional calculation, illustrates accurate modeling of the physical experiment.[12]

Assuming that the Sampath and Wilbur value of 450 deg Celsius represents three significant figures, and that the source input for ATHERMAL*2 is relatively accurate, the effect of radial heat conduction is clear.[12] This effect is depicted in Figure 9 where the radial surface temperature for a 0.50cm radius beam is plotted. The influence of radial heat conduction from the stainless steel target to the copper holder is readily apparent. From the t=2.25 seconds "snapshot" of Figure 9, the temperature at r=0 (the centerline) is 230 deg Celsius, and at r=0.27cm the temperature is 65 deg Celsius, whereas at r=0.47cm the temperature is 24 deg Celsius. At t=11.0 seconds, T(r=0)=446 deg Celsius, T(r=0.27cm)=271 deg Celsius, and T(r=0.47cm)=176 deg Celsius. Figure 9 shows that an actively-cooled target holder, which is modeled as a constant temperature boundary, has a significant effect on conducting heat from the target radially. As previously discussed, the full impact of this effect is probably not accurately reflected in these results because of the problem with the heat source input to ATHERMAL*2.

Figure 9. Radial Surface Temperature Distribution (11 sec. deposition)

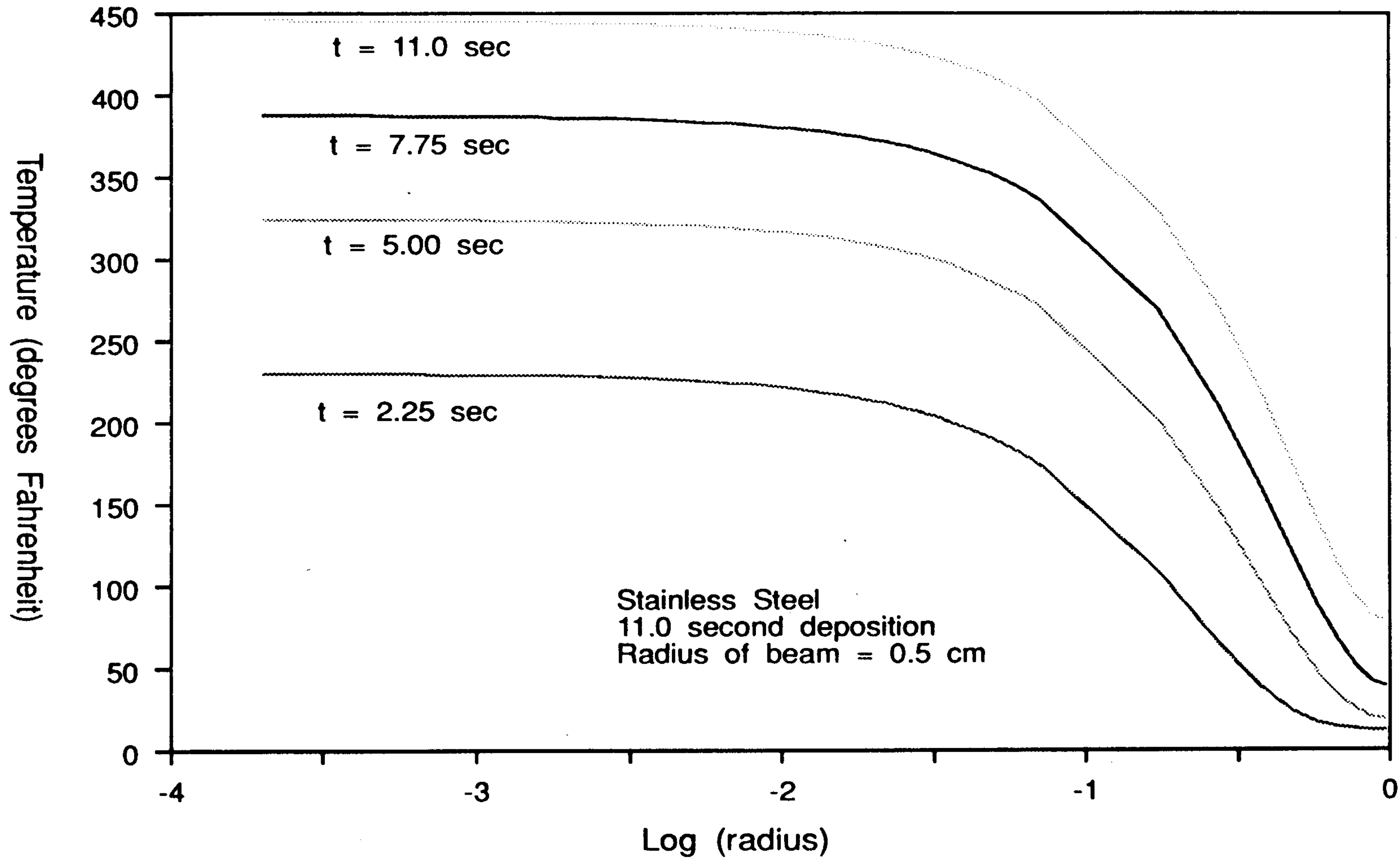

However, the overall physical behavior is relevant to accurately modeling this beam-target interaction.

The dependence of the surface temperature on the area exposed during ion implantation was also investigated; Figure 10 illustrates the results. Earlier it was noted that for a beam radius equal to 0.48cm, 0.50cm, and 0.52cm the maximum centerline surface temperature for an 11.0 second deposition is 444 deg Celsius, 446 deg Celsius, and 447 deg Celsius, respectively. This trend is expected, and if the boundary condition for the target/holder interface was changed to reflect an insulated boundary condition similar to the centerline boundary condition, then the two-dimensional model would essentially be converted into a one-dimensional model.

An error is also introduced into the calculation by approximating the experimental target/holder configuration with a cylindrical geometry. Note that in the cylindrical geometry approximation depicted in Figure 7 the heat contained in the area defined by the center point of the cylinder out to a distance of 0.25cm is much further from the copper heat sink than any point in the rectangular target geometry above it. Therefore, the influence of the copper, held at constant temperature to model active cooling, is much less in this center region and will result in a higher centerline temperature. Additionally, the maximum radius of the target was taken to be 0.96cm rather than 0.87cm. Consequently, heat at the center of the target must be conducted through a greater amount of stainless steel prior to reaching the copper interface. Since the conductivity of stainless steel is much less than that of copper, heat is not being conducted out of the target as

Figure 10. Radial Surface Temperature Distribution: Various Beam Radii (11 sec. deposition)

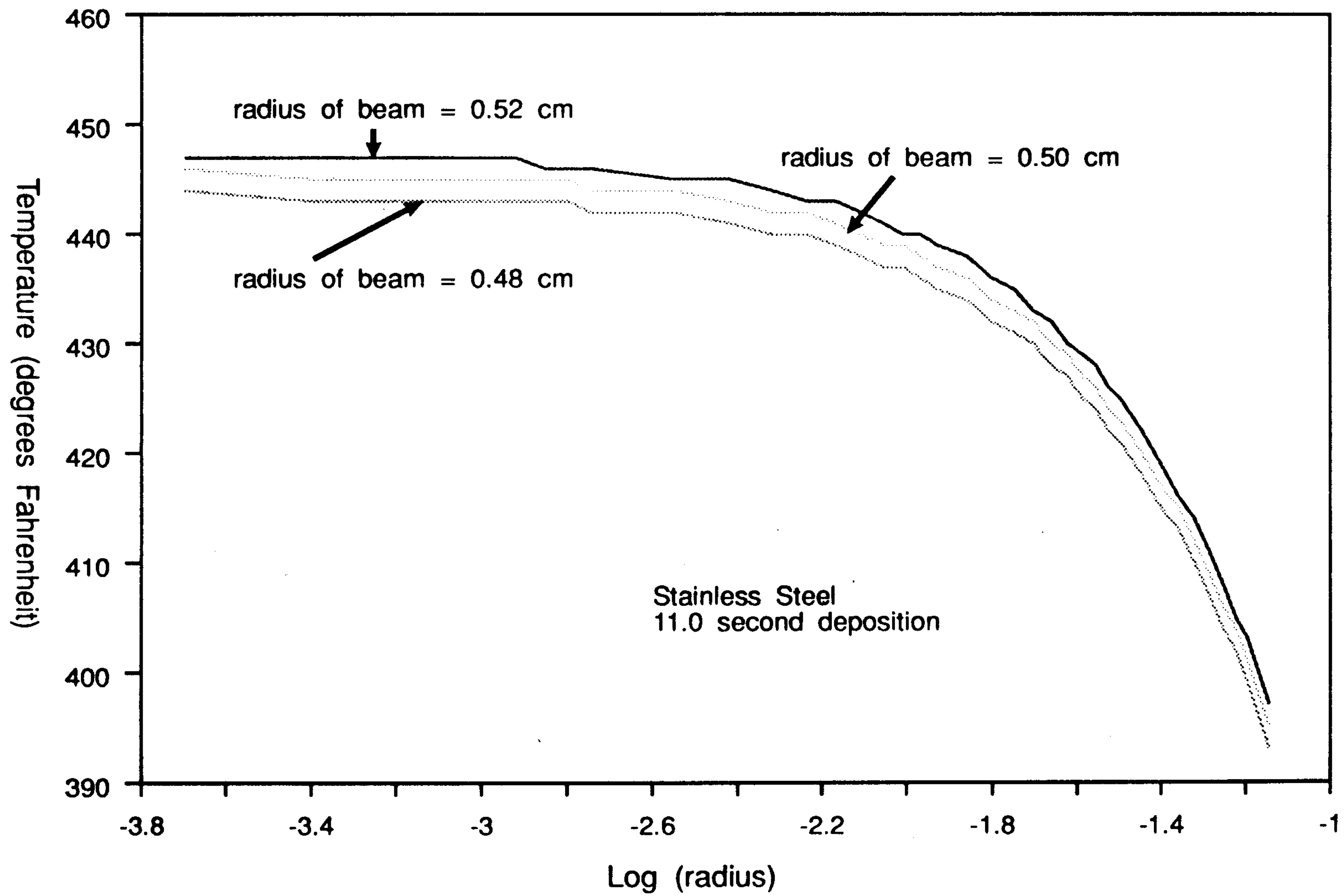

rapidly, and therefore the centerline surface is probably higher than it actually should be.

Included in the Sampath and Wilbur article is a table depicting the effect of ultrahigh current density nitrogen ion implantation on bulk hardness.[12] For the stainless steel sample the implantation current density and the energy per ion are 1500 uA/cm^2 and 60 keV, respectively. However, the total dose is listed to be $1.6x10^{17}$ $ions/cm^2$, somewhat higher than the total dose of $1.0x10^{17}$ alluded to in the surface temperature discussion of the article, and assumed in the previously described ATHERMAL*2 calculation. The duration of the implantation is not mentioned, and therefore it is assumed that this total dose, $1.6x10^{17}$ ions/cm2, denotes an implantation lasting longer that 11.0 seconds. From equation 5.6 it is known that the energy density is roughly 990 J/cm^2. Then using equation 5.5, the total dose can be written as,

$$\text{Total dose} = (990J/cm^2)/(60keV/ion)(1.60219x10^{-19}J/ev) \qquad 5.7$$

and

$$\text{Total dose} = 1.03x10^{17}\ ions/cm^2 \qquad 5.8$$

which is "approximately" the $1x10^{17}$ $ions/cm^2$ noted in the article.[12] Subsequently, the dose rate, or implantation rate, is simply,

$$\text{Dose rate} = (1.03x10^{17}\ ions/cm^2)/(11.0\ seconds) \qquad 5.9$$
$$= 9.36x10^{15}\ ions/cm^2\text{-}sec$$

Therefore, the duration of an implantation, defined by the same current density and ion energy, to deposit a total dose of $1.6x10^{17}$ $ions/cm^2$ is,

$$\text{Deposition time} = (1.6\text{x}10^{17}\text{ions/cm}^2)/(9.36\text{x}10^{15}\text{ions/cm}^2\text{-sec}) \quad 5.10$$

$$= 17 \text{ seconds}$$

Figure 11 shows that results of a 17 second deposition (1500 uA/cm2 current density and 60 keV ion energy) for three separate beam radii. The maximum centerline surface temperature for beam radii of 0.48cm, 0.50cm, and 0.52cm was calculated to be 529 deg Celsius, 532 deg Celsius, and 535 deg Celsius, respectively, still well below that melting point of 1427 deg Celsius for stainless steel. Figure 12 shows the radial surface temperature distribution for this case.

Figure 11. Centerline Surface Temperature (17 sec. deposition)

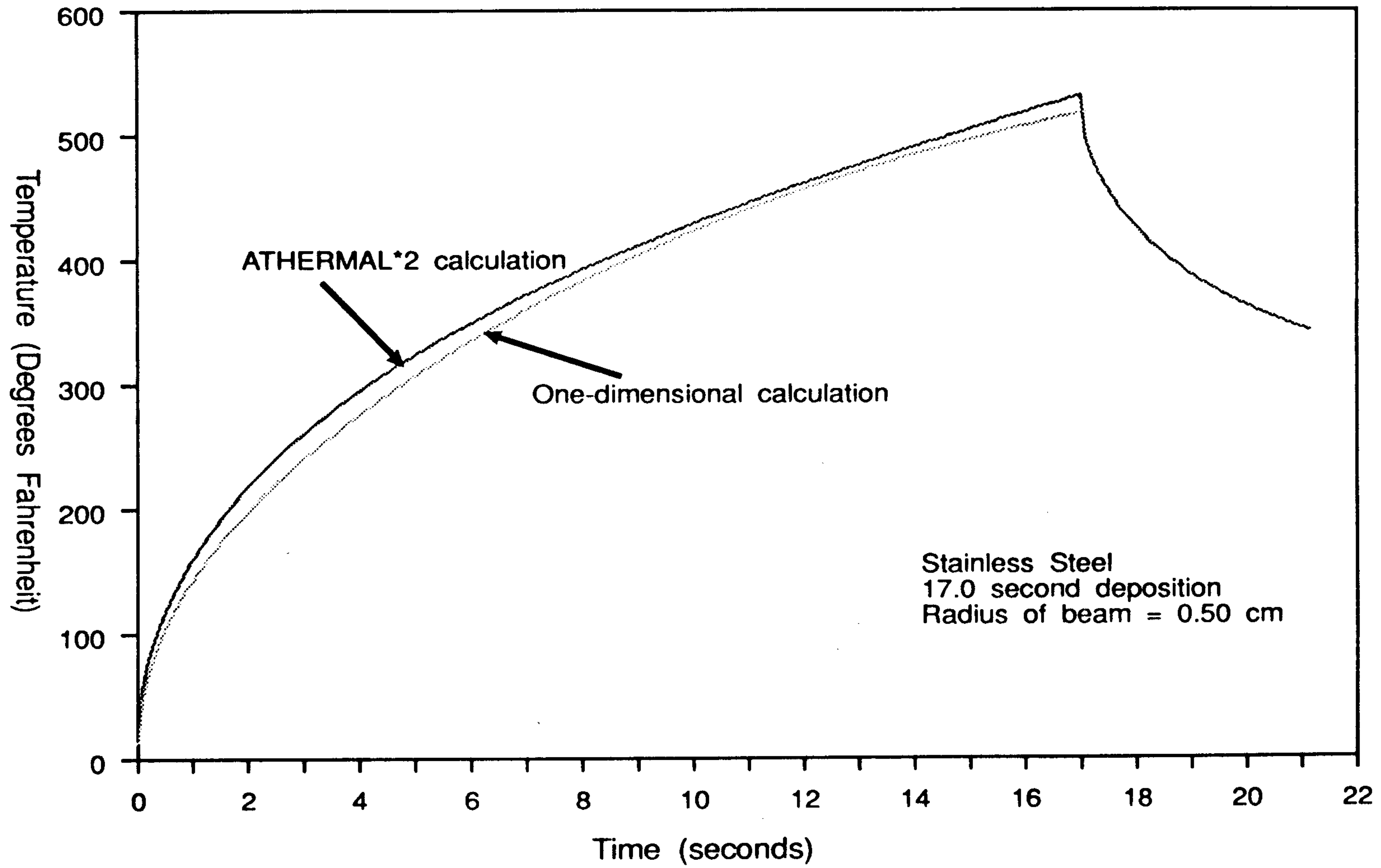

Figure 12. Radial Surface Temperature Distribution (17 sec. deposition)

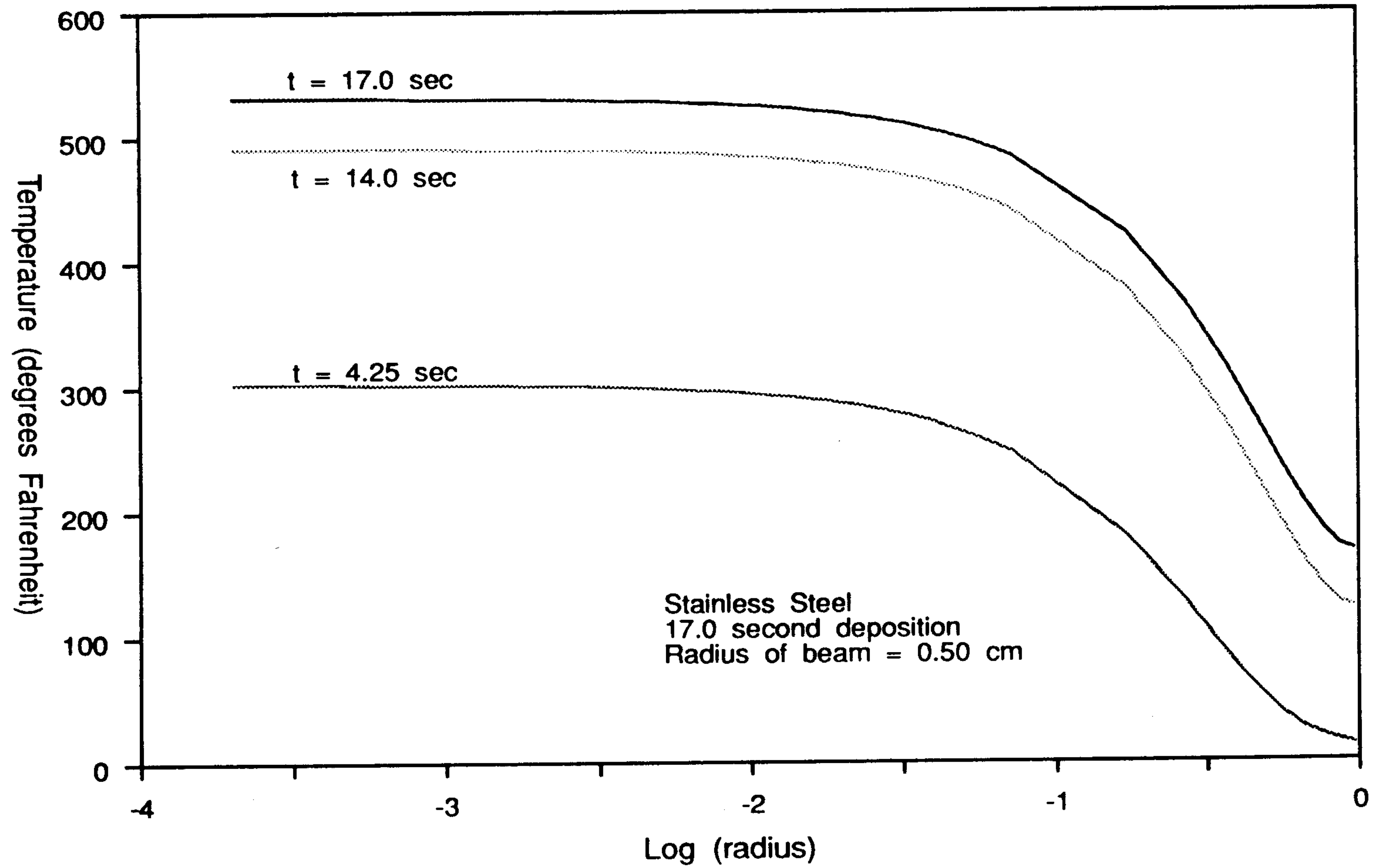

VI. CONCLUSION

It has been shown that the computer code, ATHERMAL*2, developed to model plasma disruptions and subsequent energy deposition on a fusion reactor first wall can be used to calculate surface and bulk temperatures information during ion implantation. For the particular cases that were modeled, a one-dimensional calculation appears to be adequate on a macroscopic level when determining whether the target may approach temperatures that denote the onset of bulk material property changes. Additionally, this model appears adequate for roughly calculating the duration for which the target material remains above these temperature levels. Furthermore, researchers have noted that with high current density implantation, temperature excursions exceeding transformation values for tempering and annealing will likely result, but that if the elapsed time the sample is above this transformation temperature is insufficient for nucleation and growth reactions then the bulk properties will be unaffected.[12] With the two-dimensional model, and some characterization of a material's bulk property transformation regime, researchers could refine dose estimates. In turn, manufacturers could push limits of dose rate and duration, potentially enhancing the ion implantation effects. The impact of using a two-dimensional model could be most important during the cooling phase since it incorporates radial heat conduction, and thus will more accurately characterize an actively cooled target holder. The two-dimensional model also allows researchers to calculate the effect of various target holder cooling schemes by altering the boundary condition.

The two-dimensional model may also prove to be a useful tool for metallurgists attempting to control the temperature of the solid during implantation so that ions could be implanted into crystal positions which would not form had impurities been added at an earlier melt stage in the crystal growth. Moreover, if too much energy is delivered the inclusion of the moving boundary in the calculation may be useful to ascertain the extent of damage to the target and possibly to the entire implantation apparatus due to melting and sputtering. In the future there may also be some application where melting, and subsequent solidification during implantation, is useful to modify surface characteristics.

References

1. Appleton, B.R., "Surface Modification of Solids", Journal of Materials for Energy Systems, 6 (3), 200-211 (December 1984).

2. Picraux, S.T., "Ion Implantation Metallurgy", Physics Today, 37 (11), 38-44 (November 1984).

3. Basta, N., "Ion-Beam Implantation", High Technology, 5 (2), 57-59, 61 (1985).

4. Smidt, F.A., "Recent Advances in the Application of Ion Implantation to Corrosion and Wear Protection", Nuclear Instruments and Methods in Physics Research B10/11, 532-538 (1985).

5. Dearnaley, G., "Applications of Ion Implantation in Metals", Thin Solid Films 107, 315-326 (1983).

6. Drozda, Thomas J., "Ion Implantation", Manufacturing Engineering, 94 (1), 51-56 (January 1985).

7. Cassidy, V.M., "Ion Implantation Process Toughens Metalworking Tools", Modern Metals, 40 (8), 65-67 (September 1984).

8. Sioshansi, P., "Ion Beam Modification of Materials for Industry", Thin Solid Films 118, 61-71 (1984).

9. Williams, J.M., "Wear Improvement of Surgical Ti-6Al-4V Alloy by Ion Implantation", Nuclear Instruments and Methods in Physics Research, B10/11, 539-544 (1985).

10. Singer, I.L., Bolster, R.N., Sprague, J.A., Kim, K., Ramalingam, S., Jefferies, R.A., and Ramseyer, G.O., "Durable Metal Carbide Layers on Steels Formed by Ion Implantation at High Temperatures", Journal of Applied Physics, 58 (3), 1255-1258 (August 1985).

11. Follstaedt, D.M., "Implantation of Ti+C for Reduced Friction and Wear of Steels", Nuclear Instruments and Methods in Physics Research, B10/11, 549-555 (1985).

12. Sampath, W.S. and Wilbur, P.J., "Broad Beam Ultrahigh Current Density Ion Implantation", Material Research Society Symposium Proceedings, 93, 349-360 (1987).

13. Woodard, O., Lindsey, P., Cecil, J., and Pipe, R., "Computer Automation of High Current Ion Implanters", Nuclear Instruments and Methods in Physics Research, B6, 146-153 (1985).

14. Smidt, F.A., Sartwell, B.D., and Bunker, S.N., "U.S. Navy Manufacturing Technology Program on Ion Implantation", Materials Science and Engineering, 90, 385-397 (1987).

15. Carnahan, B., Luther, H.A., and Wilkes, J.O., Applied Numerical Methods, John Wiley & Sons, New York (1969).

16. Robinson, A.H., Notes for ME 575 #1 - Transient Heat Conduction, Oregon State University, Corvallis, OR (Fall 1990).

17. Hassanein, A.M., private communications, Argonne National Laboratory, Argonne, IL, (1986-1990).

18. Hassanein, A.M., "Simulation of Plasma Disruption Induced Melting and Vaporization By Ion or Electron Beam", Journal of Nuclear Materials, 122 & 123, 1453-1458 (1984).

19. Hassanein, A.M., Kulcinski, G.L., and Wolfer, W.G., "Surface Melting and Evaporation During Disruptions in Magnetic Fusion Reactors", Nuclear Engineering and Design/Fusion, 1, 307-324 (1984).

20. Hassanein, A.M., Kulcinski, G.L., and Wolfer, W.G., "Vaporization and Melting of Materials in Fusion Devices", Journal of Nuclear Materials, 103 & 104, 321-326 (1981).

21. Hassanein, A.M., Kulcinski, G.L., and Wolfer, W.G., "Dynamics of Melting, Evaporation, and Resolidification of Materials Exposed to Plasma Disruptions", Journal of Nuclear Materials, 111 & 112, 554-559 (1982).

22. Smith, T.C., "Wafer Cooling and Photoresist Masking Problems in Ion Implantation", Ion Implantation: Equipment & Techniques, Ryssel & Glawischnig editors, Springer-Verlag, New York (1983).

23. Robinson, A.H., private communications, Oregon State University, Corvallis, OR (1990).